ChemSusChem

Research Article
doi.org/10.1002/cssc.202300445

Chemistry Europe
European Chemical Societies Publishing

www.chemsuschem.org

Special Collection

Evaluating a Dual-Ion Battery with an Antimony-Carbon Composite Anode

Thrinathreddy Ramireddy,[a, b] Jens Matthies Wrogemann,[c] Lukas Haneke,[c] Irin Sultana,[d, e] Felipe Kremer,[f] Ying Ian Chen,[d] Martin Winter,[c, g] Tobias Placke,*[c] and Alexey M. Glushenkov*[a, b]

Dual-ion batteries (DIBs) are attracting attention due to their high operating voltage and promise in stationary energy storage applications. Among various anode materials, elements that alloy and dealloy with lithium are assumed to be prospective in bringing higher capacities and increasing the energy density of DIBs. In this work, antimony in the form of a composite with carbon (Sb–C) is evaluated as an anode material for DIB full cells for the first time. The behaviour of graphite||Sb–C cells is assessed in highly concentrated electrolytes in the absence and presence of an electrolyte additive (1% vinylene carbonate) and in two cell voltage windows (2–4.5 V and 2–4.8 V). Sb–C full cells possess maximum estimated specific energies of 290 Wh/kg (based on electrode masses) and 154 Wh/kg (based on the combined mass of electrodes and active salt). The work expands the knowledge on the operation of DIBs with non-graphitic anodes.

Introduction

The power generation and transportation sectors are major contributors to greenhouse gas emissions. The transition from fossil fuel power generation to renewable energy and from internal combustion engine vehicles to electric vehicles (EVs) are the key developments to meet the targets set by the United Nations on climate change. The on-going transition is evident, for example, from a recent two-fold increase in the sales of EVs (almost 6.7 million vehicles sold in 2021 in comparison wth 3.2 million vehicles sold in 2020).[1] Similarly, the global electricity generated from renewable resources accounted for 29%, i.e., 632 TWh, in 2020–21, an increase of 23.7% compared to 2019–20.[2] Importantly, solar photovoltaics and wind accounted for 66.4% of total renewable energy in 2020–21 and are predicted to grow their importance further in the next decade. The renewable energy generation of this nature is intermittent and requires an electrochemical energy storage device to store the energy for off & on-grid systems. Lithium-ion batteries (LIBs) quickly penetrate into the grid application as energy systems of choice due to their high energy and power density. However, considering the predicted upside in the use of battery storage and a limited availability of some of the resources (e.g., lithium, cobalt and nickel minerals and salts) required for LIBs, a price rise similar to the oil price increases in the past may be envisaged. Henceforth, researchers are looking for viable alternatives to LIBs in applications where space is not a constraint, including grid-level energy storage. In this regard, various metal-ion batteries such as Na-ion,[3] K-ion,[4] Ca-ion,[5] Al-ion,[6] and Mg-ion batteries,[7] with working principle similar to that of LIBs (rocking chair mechanism), are intensely researched at present. In the interim, a different battery concept, a dual-ion battery (DIB), has also gained much attention due a range of inherent benefits, including their superior environmental friendliness, the lack of need for expensive transition metals in their positive electrodes, and the

[a] Dr. T. Ramireddy, Prof. A. M. Glushenkov
Research School of Chemistry
The Australian National University
Canberra, ACT 2601 (Australia)
E-mail: alexey.glushenkov@anu.edu.au

[b] Dr. T. Ramireddy, Prof. A. M. Glushenkov
Battery Storage and Grid Integration Program
The Australian National University
Canberra, ACT 2601 (Australia)

[c] J. M. Wrogemann, L. Haneke, Prof. M. Winter, Dr. T. Placke
MEET Battery Research Center
University of Münster
Corrensstraße 46, Münster 48149 (Germany)
E-mail: tobias.placke@uni-muenster.de

[d] Dr. I. Sultana, Prof. Y. Ian Chen
Institute for Frontier Materials
Deakin University
Waurn Ponds, VIC 3216 (Australia)

[e] Dr. I. Sultana
School of Materials and Energy
Guangdong University of Technology
Guangzhou, Guangdong 51006 (P. R. China)

[f] Dr. F. Kremer
Centre for Advanced Microscopy
The Australian National University
Canberra, ACT 2601 (Australia)

[g] Prof. M. Winter
Helmholtz Institute Münster
IEK-12
Forschungszentrum Jülich GmbH
Corrensstraße 46, Münster 48149 (Germany)

Supporting information for this article is available on the WWW under https://doi.org/10.1002/cssc.202300445

Special Collection This publication is part of a collection of invited contributions focusing on "Dual-Ion Batteries". Please visit chemsuschem.org/collections to view all contributions.

possibility to deploy low-cost carbonaceous materials (especially graphite) instead.[8]

DIBs operate differently to LIBs. During the charging process, the anions from the electrolyte salt intercalate into the graphite positive electrode in such a battery while the cations are inserted into the negative electrode. When an external curcuit is connected to battery terminals, the reverse process occurs inside of the cell, and the electron flow is created to power the external circuit. Unlike LIBs, the ions in the electrolyte of DIBs should be considered as active materials in addition to the materials of electrodes, as they are consumed by electrodes and released back into the electrolyte in each cycle. A very notable difference with LIBs is the requirement of anion insertion in the positive electrode.[8] In their early contribution in 1938, Rüdorff and Hoffman demonstrated the reversible insertion of anions into graphite.[9] Recently, other materials such as organic polymers,[10] metal-organic frameworks,[11] and conversion materials[12] have also been studied as positive electrode materials for DIBs. However, a significant advantage of graphite is its ability to host a large variety of anions such as PF_6^-,[13] BF_4^-,[14] FSI^-,[15] $TFSI^-$,[16] $FTFSI^-$,[16] and ClO_4^-,[17] and a high operating potential (4.5–5.2 V vs. $Li|Li^+$) at which insertion of such anions occurs. Depending on the intercalating anion, reversible capacities up to 120 −140 mAh/g can be obtained. The choice of an electrolyte is also crucial; due to a high insertion potential of graphite electrodes, the electrolyte should have high oxidation stability to enable an enhanced Coulombic efficiency. Recent studies have indicated that the use of highly concentrated electrolytes (HCEs) such as 4 M $LiPF_6$ or 3.4 M LiTFSI in dimethyl carbonate (DMC) leads to a better cyclic performance and suppresses the dissolution of aluminium current collector. Consequently, HCEs can often be preferred for evaluating the performance of DIBs.[8,13b]

Graphite has been widely used as an anode material in commercial LIBs. However, some known disadvantages of this material are its low gravimetric capacity of 372 mAh/g, and a low tap density (a metric affecting volumetric capacity).[18] The other major disadvantage of graphite is its low operating potential (<0.2 V vs. $Li|Li^+$), which may lead to Li metal dendrite formation on the surface of the electrode under harsh charging conditions. In particular, when graphite is used in a DIB instead of a LIB, the passivation of electrolyte on the cathode surface may force the potential of the negative electrode to reach plating region, with serious safety issues. One possible strategy to deal with the drawbacks of graphite as an anode material in DIBs is replacing it with anode materials that participate in an alloying reaction mechanism with lithium. Such materials, most notably, silicon, have been considered in the past to improve LIBs and push their energy density boundaries, and numerous start-up companies are actively pursuing the commercialisation of Si-based battery systems.[19] It may be envisaged, that the benefits of the alloying anode materials may also be applicable to DIBs. In particular, these materials (including Si, Sb, P, Bi and Al) have high gravimetric capacities (2 to 10 times greater than that of graphite), and attractive volumetric capacities. Traditionally, the major challenge associated with the alloying materials was a significant volume change during lithiation/de-lithiation.[20] However, an approach consisting of mixing the active phases in the form of nansocale particles with a carbon matrix has been proven effective to mitigate this unusual volume variation in recent experiments, and a reasonable, stable cyclic behaviour can be achieved in many studies.[18]

Even though alloying materials possess enormous capacities, their practical evaluation in DIBs is necessary and limited at present. In this regard, only some candidates belonging to this class of anode materials, in the form of appropriate composites with carbon such as Si – carbon,[21] Ge – carbon nanofibers,[22] and Al – carbon,[23] have been evaluated as anodes for DIBs. Recently, we investigated DIBs involving black phosphorus (black P) – carbon composites, in the form of cells assembled using a 1:1.2 capacity balancing ratio (cathode to anode capacity ratio). The cells exhibited specific energy 319 Wh/kg based on the mass of active materials in two electrodes, or 155 Wh/kg based on the combined mass of electrode active materials and active salt.[24] Obviously, it is important to expand the experimental screening of the available alloying materials in DIBs to the materials not assessed yet as well. In this context, antimony (Sb) represents another interesting candidate material with the theoretical capacity of 660 mAh/g.[25] Similar to phosphorus, antimony alloys and dealloys with lithium at a higher operating potential (1.2–0.6 V), preventing dendrite formation, and is able to demonstrate excellent cyclic stability, depending on the preparation conditions. To the best of our knowledge, Sb-based composite materials have not been evaluated in DIBs so far.

Herein, we report Li-based DIBs using an antimony-carbon composite (Sb–C) anode for the first time. The composite material is synthesised using a ball milling technique with bulk Sb and graphite powders as starting materials. Initially, this Sb–C composite material is evaluated for its electrochemical performance in Li metal cells using different HCEs. Subsequently, the Sb–C composite electrodes are paired against the graphite cathodes. The corresponding full-cell behaviour is investigated using 3.4 M LiTFSI in DMC electrolyte and a three-electrode setup to monitor the performance of both electrodes. The electrode balancing ratio is chosen as 1:1.1 (a ratio of cathode capacity to anode capacity), similar to the industrial standards typically used for LIBs. The key performance metrics, such as the specific capacity and Coulombic efficiency (C_{EFF}), are evaluated for different cell potential windows, and the specific energy of DIBs is compared to those of dual-graphite batteries. Furthermore, the usage of electrolyte additive such as vinylene carbonate (VC) is explored. It is shown that the VC additive increases the cyclic stability but leads to potential safety issues (Li metal plating). Building on the previous literature, this study provides vital information about the applicability and choice of anode materials with an alloying reaction mechanism for the design of DIB full cells.

Results and Discussion

Structural Characterisation of the Antimony – Carbon Composite

An antimony-carbon composite used as the anode material was characterised by X-ray diffraction (XRD), Raman spectroscopy and transmission electron microcsopy (TEM). The XRD pattern of the Sb–C composite is shown in Figure 1a, and most of the reflections in the pattern coincide with the expected reflections of the Sb phase in the standard diffraction card (Inorganic Crystal Structure Database card no # 98-006-4695). The reflections originating from the Sb are somewhat broadened but still relatively sharp, indicating that no phase change and some (but not extreme) crystal size change occurred in the material upon mechanical milling. In addition to the set of Sb peaks, a small single reflection at 26.4° corresponds to the (002) reflection from graphite (ICSD card no # 98-007-6767). Other reflections of graphite are not visible. This reflection demonstrates that the graphitic structure still exists in the carbon component of the sample. However, ball milling introduces structural modification and local disordering in the graphite upon milling process. Figure 1b shows the Raman spectra of the Sb–C composite. Two bands recorded around 108 cm^{-1} and 145 cm^{-1} are associated with E_g and A_{1g} bands of the Sb phase.[26] Moreover, there is a broad peak around 230–289 cm^{-1} ascribed to second-ordered phonon scattering of optical phonon 2 A_{1g} of Sb.[26a] Consistent with our previous report,[27] the strong intensity of Sb peaks suggests the presence of Sb particles in the composite. Another three bands, a characteristic signature of graphite, are recorded around 1343, 1578 and 2688 cm^{-1}, and correspond to D, G, and 2D bands of graphite, respectively. The G band originates from the E_{2g} vibration mode, which occurs due to the relative motion of sp^2 carbon atoms. The D band represents the breathing mode and is inhibited in the graphitic structure but occurs in disordered graphite. The intensity of the D/G band ratio is widely used to assess the disordered structure of the graphite. The I_D/I_G ratio in this materials is greater than 1, whereas for commercial graphite it is around 0.16 (S.I. Figure S1). It may indeed be expected that, during milling, large graphite particles are broken down into small clusters, flakes and sheets with a significant amount of structural defects. In the context of a Raman spectrum, the above actions cause the widening of the G band and an increase of the D band in the Raman spectra. Similarly, ball milling breaks the weak Van der Waals band between the basal planes and destroys the original ordering of the basal plane along the c-axis, thereby reducing the thickness of graphite fragments. This can be inferred from the widened 2D band coupled with a reduced intensity obtained from the Sb–C composite, in comparison with the commercial graphite.

The results of TEM characterisation are shown in Figure 1c, d. A TEM image of the composite material is presented in Figure 1c. Figure 1d shows an overlap of elemental maps of Sb

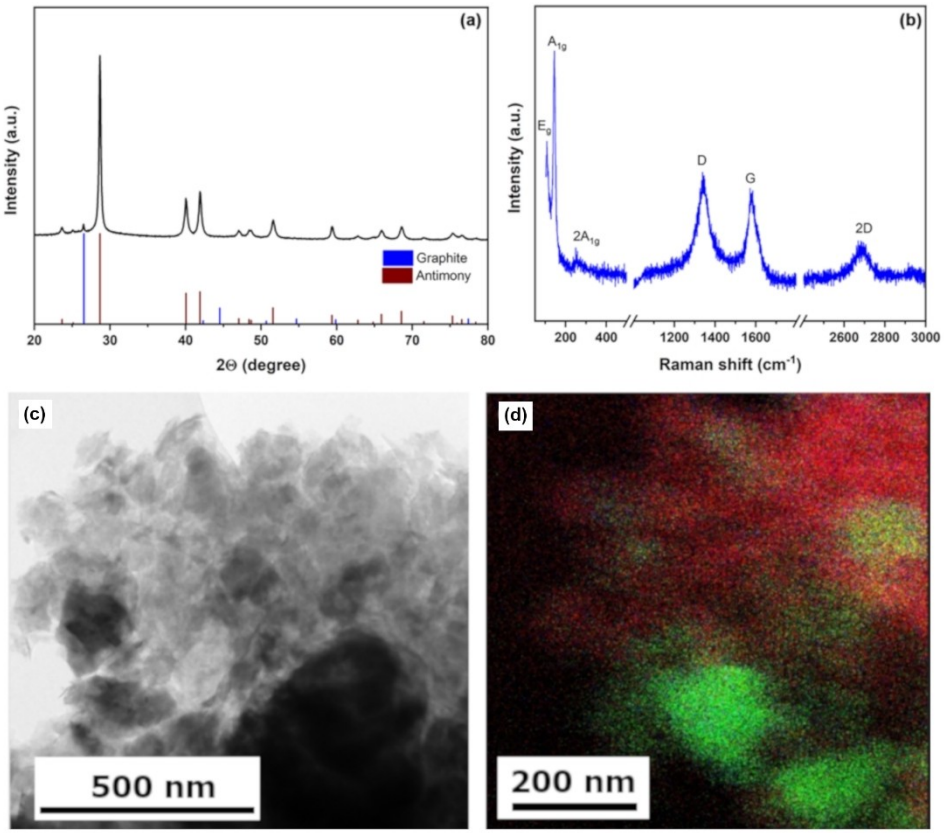

Figure 1. Structural characterisation: (a) XRD pattern; (b) Raman spectrum of the Sb–C composite; (c, d) TEM image and overlay of Sb (green) and C (red) energy-dispersive EDX maps of the sample.

(green) and C (red). It can be noted that both relatively large (up to 200 nm in size) and very fine Sb particles are present. The fraction of smaller particles is well intermixed with the carbon co-component of the composite, in line what was observed elsewhere.[27] As we discussed in our previous publication, the size distribution of the Sb particles depends on the milling condition, and the observations in Figure 1c,d are consistent with the milling mode applied in the preparation of the composite. Overall, it is confirmed that the sample contains Sb particles on a nanometre scale at least partially intermixed with carbon component. Some of the carbon remains in the form of graphite used as a precursor for milling.

Electrochemical Performance Optimisation of the Antimony – Carbon Composite against Lithium Metal

The synthesised Sb–C composite material was evaluated for its electrochemical performance in Sb–C || Li metal cells to evaluate the best electrolyte and separator for the fabrication of a graphite || Sb–C full cell. The literature suggests that DIBs show a better performance in terms of capacity and cyclic stability in highly concentrated electrolytes (HCEs).[13b,28] Therefore, the electrodes were tested in HCEs, but initially their electrochemical performance was also assessed in a commercial lithium-ion battery electrolyte (1 M of $LiPF_6$ EC:EMC in 1:1 vol. ratio; S.I. Figure S2a) as a control experiment. Consistently with our previous work,[29] the electrodes were pressed and tested under a constant current rate of 229 mA/g. Polyolefin non-woven FS 2226 separator (Freudenberg) was used. This cell, tested using a commercial electrolyte, shows an initial discharge capacity of 557 mAh/g, which is close to the theoretical capacity of approximately 574 mAh/g for the Sb–C composite (assuming that the capacity of carbon is similar to that of graphite). What can be seen from Figure S2 is that the electrode shows a steep decline in capacity in the first five cycles, which is followed by a gradual decrease until the end of 100 cycles. The electrode retains 65.6% of the initial capacity in the 100th cycle. The Coulombic efficiency of an individual electrode is also important, as it may determine the capacity retention and cyclic stability of DIBs. The electrode shows an initial C_{EFF} of 74.7%, with an increase to 95.8% in the second cycle, and maintains C_{EFF} above 97% during the rest of the cycling period (S.I. Figure S2a). In order to evaluate electrodes in HCEs, two cells were constructed for each experiment to assess consistency, and the average capacity was plotted with a standard deviation. When 3.4 M LiTFSI in DMC electrolyte is used, the Sb–C composite electrode exhibits an initial de-lithiation capacity of only 157 mAh/g, dramatically less than the capacity of the commercial electrolyte. Furthermore, the material shows an inferior capacity retention of 56.6% after 100 cycles (S.I. Figure 2a). Our analysis indicates that an inferior capacity of the material in this test may be attributed to pressing (calendaring) of the electrode. The average porosity of the electrodes before and after pressing is 77.6% and 56.4%, respectively. The details of the porosity measurement are provided in the experimental section and S.I. Indeed, an unpressed electrode shows an enhanced initial charge capacity of 484.6 mAh/g with a capacity retention of 58.8% over the same cyclic period. The material displays a slightly reduced initial C_{EFF} of 63% compared with the commercial electrolyte, which increases to 93.8% in the seventh cycle, and maintains a stable C_{EFF} above 98% for 100 cycles (S.I. Figure 2b). The negative effect of pressing an electrode in these tests may relate to high viscosity of a HCE and an increased wetting time of the electrode.[30] The pressing of the electrode reduces porosity whereas the pores in unpressed electrodes are not blocked, thereby enhancing the penetration and electrolyte/electrode interaction area. Therefore, unpressed electrodes showed better electrochemical performance than pressed electrodes and were used for further studies.

The electrochemical performance and the C_{EFF} of the Sb–C composite in two HCEs are shown in Figure 2a. The initial capacity of the Sb–C composite material tested in 4 M $LiPF_6$ in DMC is 340 mAh/g, less than that in the cells operated using 3.4 M LiTFSI in DMC electrolyte. Additionally, the Sb–C composite material shows an increased cyclic stability in 3.4 M LiTFSI in DMC with a capacity retention of 76.8% (compared with the fourth cycle), whereas the analogous capacity retention in 4 M $LiPF_6$ in DMC is 70.5%. Due to the formation of the solid electrolyte interphase (SEI) at the electrode/electrolyte contact surface during the initial cycles, the capacity retention was compared with the fourth cycle. Coulombic efficiency in the LiTFSI-based electrolyte is also superior, the material displays an initial C_{EFF} of 63% in 3.4 M LiTFSI in DMC, whereas the electrode shows a poor initial C_{EFF} of only 31.9% in 4 M $LiPF_6$ in DMC. The C_{EFF} increases with the cycle number. The C_{EFF} in 3.4 M LiTFSI in DMC increases to above 94% in the eighth cycle and displays a stable C_{EFF} until the 30th cycle, further gradually increases to 97% in the 75th cycle, and reaches 97–98% in the end of 100 cycles in 4 M $LiPF_6$ in DMC electrolyte. The SEI formation on the surface of the electrode will be different in the presence/absence of ethylene carbonate, a cyclic ester commonly used in commercial electrolytes.[31] A possible assumption might be the formation of an unstable SEI layer on the electrode surface in the absence of ethylene carbonate in the recipe of the highly concentrated 4 M $LiPF_6$ in DMC electrolyte. However, a detailed investigation on the SEI layer particularities in HCEs is beyond the purpose of this study.

Although there is a marked increase in the electrode capacity using 3.4 M LiTFSI in DMC, the values are still less than those obtained in the commercial electrolyte. Some of this effect was traced to the nature of the separator used in Li metal cells. Figure 2b shows the results of experiments with two different separators (Freudenberg FS 2226 used in the already described experiments and Whatman GF/D glass fiber membrane). The Sb–C composite material tested using the Whatman GF/D separator in 3.4 M LiTFSI in DMC exhibits an initial capacity of around 604.6 mAh/g, almost 120 mAh/g in excess of cells assembled using the FS 2226 separator. The material retains a capacity of 71.3% in the end of 100 cycles using the GF/D separator, slightly inferior to the capacity retention with the FS2226 separator (76.8%). The capacity retention in both cases is calculated against the capacity obtained in the fourth

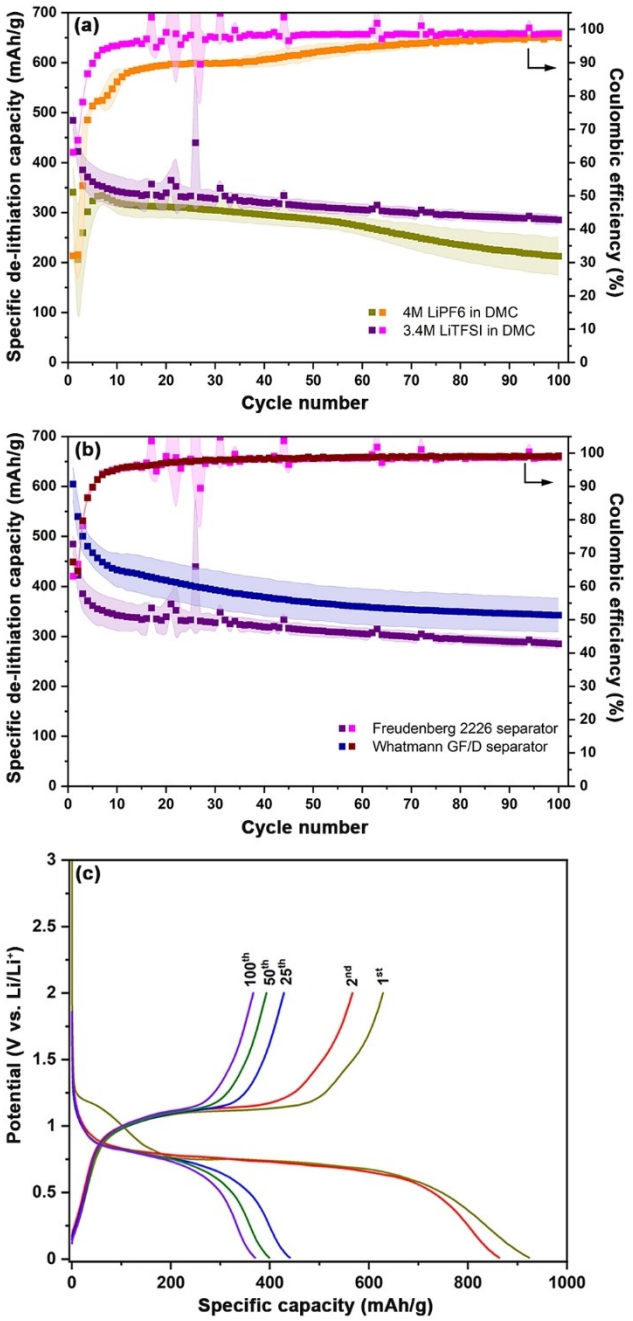

Figure 2. Electrochemical performance of Sb–C | | Li metal cells: (a) delithiation capacity and Coulombic efficiency vs. cycle number in highly concentrated electrolytes with Freudenberg FS 2226 separators; b) delithiation capacity and Coulombic efficiency vs. cycle number in 3.4 M LiTFSI in DMC electrolyte with two different separators (Freudenberg FS 2226 and Whatman glass fiber GF/D); c) discharge and charge profiles for various cycles in 3.4 M LiTFSI in DMC electrolyte with Whatman glass fiber GF/D separator. The electrodes were unpressed, and cells were cycled at a current rate of 0.4 C (1 C = 573.6 mAh/g).

cycle. The initial C_{EFF} is slightly higher with the GF/D separator (67.3 %) than with the FS2226 separator (63 %). The trends in the C_{EFF} increases upon cycling do not show marked differences. It has been previously demonstrated that Whatman GF/D separators show a better wettability and lead to a better ionic conductivity between electrode than with other separators, including Freudenberg FS 2190, in ionic liquids.[32] Even though the separator variants and electrolytes used in this study are dissimilar, the results show that cells employing Whatman GF/D separators exhibit faster ion transport and therefore may enable higher capacities than polyolefin-based separators. The lithiation and delithiation profiles of the Sb – carbon composite material in 3.4 M LiTFSI in DMC with a Whatman GF/D separator are shown in Figure 2c. The first cycle profiles in 3.4 M LiTFSI in DMC are similar to those in a commercial electrolyte, except for a slight increase in voltage hysteresis (S.I. Figure 2a). This clearly illustrates the charge storage mechanism in Sb–C composite material follows a similar pattern in HCEs to its usual behaviour if an electrolyte and a separator are selected correctly. It can be seen that the electrode retains consistent features in its cyclic profile for over 100 cycles, subject do the capacity decay in line with cyclic stability shown in Figure 2b. Overall, on the basis of the intial results on the capacity retention and C_{EFF}, 3.4 M LiTFSI in DMC electrolyte and GF/D separator were chosen for our full cell studies.

The Electrochemical Performance of DIB Full Cells and the Effect of Cell Voltage

To inform the fabrication of DIB full cells, the electrochemical performance of Sb–C composite (from the previous section) and graphite in Li metal cells, i.e., against lithium metal, was taken into account. The data on the electrochemical performance of graphite against lithium metal were taken from our previous work.[24] An important step in designing a full cell is to balance the capacities of the positive electrode (PE) and the negative electrode (NE) in an appropriate manner, because this has a significant effect on the working potential ranges for both electrodes. The first consideration is to avoid forcing the NE to operate at a potential at which lithium plating is possible; for this reason the NE:PE capacity ratio is maintained at above 1.[33][34] Additionally, in DIBs, the electrolyte acts as charge storage medium in the discharged state. Li metal is deposited on the NE's surface when the NE's nominal capacity is exceeded. This will lead to dendrite formation (safety issues) and capacity fade in the full cell. Conversely, a higher excess capacity (NE > PE) increases the total active mass without capacity gains coupled with a reduction in cell voltage, thereby decreasing energy density. Therefore, after a careful consideration of both safety and energy density, the NE : PE capacity ratio was maintained as 1.1 : 1. For the purposes of balancing electrodes in a full cell, the electrode capacities were determined from the third discharge and charge cycle at 0.5 and 0.4 C after the completion of formation cycles for the cathode and the anode from their Li metal cell experiments. The full cells were fabricated using a three-electrode setup to monitor the individual performance of both electrodes against a reference electrode in the form of a piece of Li metal. The cells were cycled between two different upper cut-off voltages 4.5 and 4.8 V to restrict the graphite electrode upper cut-off potential to 5.0 and 5.2 V versus Li metal reference, respectively.

The above potential windows were obtained from the individual Li metal cell results of graphite and the Sb-carbon composite.

Figure 3a shows the specific discharge capacities of graphite||Sb-carbon full cells operated with two different upper cut-off voltages. Initially, the cells were cycled at 0.1 C (10 mA/g) for the first three cycles as a part of the formation cycle protocol. Following that, the cells were charged and discharged at 50 mA/g, equivalent to 0.5 C. The capacity values represented in the figure are related to the mass of the cathode. Two cells were fabricated, and the average values were plotted along with the standard deviation. As expected, the cells operating within a wider potential window (2–4.8 V) show a higher initial capacity of 96 mAh/g during the formation cycle. The discharge capacity of the cells is reduced from 94 mAh/g (during the third cycle) to 89 mAh/g as the current rate increases from 0.1 C to 0.5 C. This effect can be correlated to voltage hysteresis, which is predictable with the increase in the current rate (S.I. Figure S4a). The capacity declines gradually and drops to 81 mAh/g after 30 cycles; this, however, is followed by an accelerating degradation to 44 mAh/g after 78 cycles. Even though the two cells exhibited somewhat different degradation behaviour (Figure 3a, note the magnitude of standard deviation), they still exhibit similar discharge capacities (approximately 44 mAh/g) after 78 cycles, and the behaviour at this point becomes much more similar and the standard deviation for the two cells becomes small. For the cells operated within a potential window of 2 and 4.5 V, a capacity of around 86 mAh/g is demonstrated in the last formation cycle. The same cells exhibit a discharge capacity of 80 mAh/g during the fourth cycle and a slow capacity decline over the successive 75 cycles is observed, leading to the retention of 81% of capacity. The evolution of C_{EFF} is shown in Figure 3b. An initial C_{EFF} of 65% and 67% is measured for the cells with the upper cell cut-off voltage of 4.8 and 4.5 V, respectively. In the end of the formation cycles, the C_{EFF} rises to 90.8% (4.8 V) and 87.9% (4.5 V). Further, the C_{EFF} continues to increase and reaches 98% (4.8 V) after 30 cycles and drops slightly to 96.9% (78th cycle) for the two types of cells. However, for the cells operated up to 4.5 V, the C_{EFF} then increased to 97% (20th cycle), and maintains its stability for the rest of the cycling period, while the Ceff for the cell with the 4.8 V upper cut-off falls. In conclusion, the graphite||Sb-carbon (SGDIB) composite full cells operated within the voltage range of 2–4.8 V exhibit a higher capacity with a poor cyclic stability, whereas the cells cycled between 2 and 4.5 V display an enhanced cyclic stability.

To understand the origin of capacity decline in the full cells, the potential profiles of positive and negative electrodes and the cell voltage for both voltage windows are displayed in Figure 4. During the first formation cycle, in the cell operating between 2 and 4.8 V, the PE reaches a maximum potential of 5.19 V vs Li|Li$^+$, whereas the Sb-carbon composite electrode reaches a minimum potential of 0.39 V vs Li|Li$^+$, which is in line with the assumptions made from the assessment of Li metal cell results. As the current rate is increased from 10 to 50 mA/g, the NE's end of charge potential decreases to 0.34 V vs Li|Li$^+$. As expected, the increase in the current rate increases the voltage polarisation; this effect is more pronounced in the Sb-carbon composite in comparison with the graphite. Henceforth, the potential of the positive electrode decreases to 5.14 V vs Li|Li$^+$ instead of the intended 5.2 V vs Li|Li$^+$ (Figure 4). As cycling progresses, the potentials of both PE and NE are reduced further (Table 1). At the end of the 75th cycle, the potential of the NE reaches 6 mV vs Li|Li$^+$, and, concurrently, the graphite electrode's end of charge potential reaches a maximum value of very close to 4.8 V vs Li|Li$^+$. In another important observation, the negative electrode is not getting completely delithiated with the increase in cycle numbers (1.07 V vs Li|Li$^+$ in the 75th cycle); the end of graphite's discharge potential is condensed further to about 3.1 V (vs Li|Li$^+$) during the same cycle. For the cells cycled between 2 and 4.5 V, the positive electrode reaches a potential of 5.06 V (vs Li|Li$^+$), and the Sb–C composite electrode decreases to 0.57 V (vs Li|Li$^+$) in the first cycle. In contrast to the cell with a wider potential window, the voltage polarisation is negligible as the current rate increased

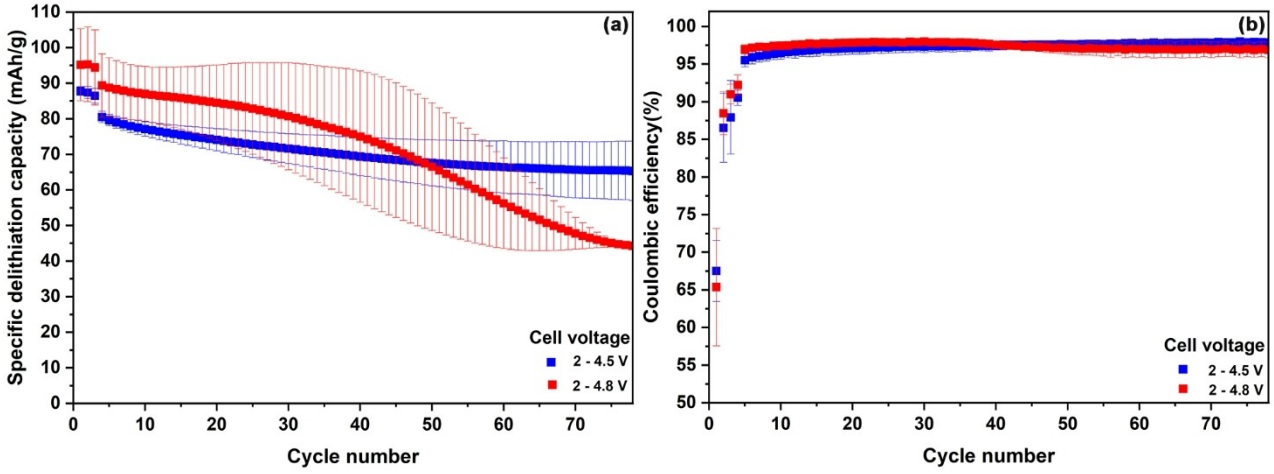

Figure 3. Electrochemical performance of graphite||Sb–C composite full cells using constant current charge-discharge testing mode: (a) specific discharge capacities as functions of the cycle number b) C_{EFF} of full cells tesed in two different cell voltage windows (2–4.3 and 2–4.5 V) with 3.4 M LiTFSI in DMC as an electrolyte.

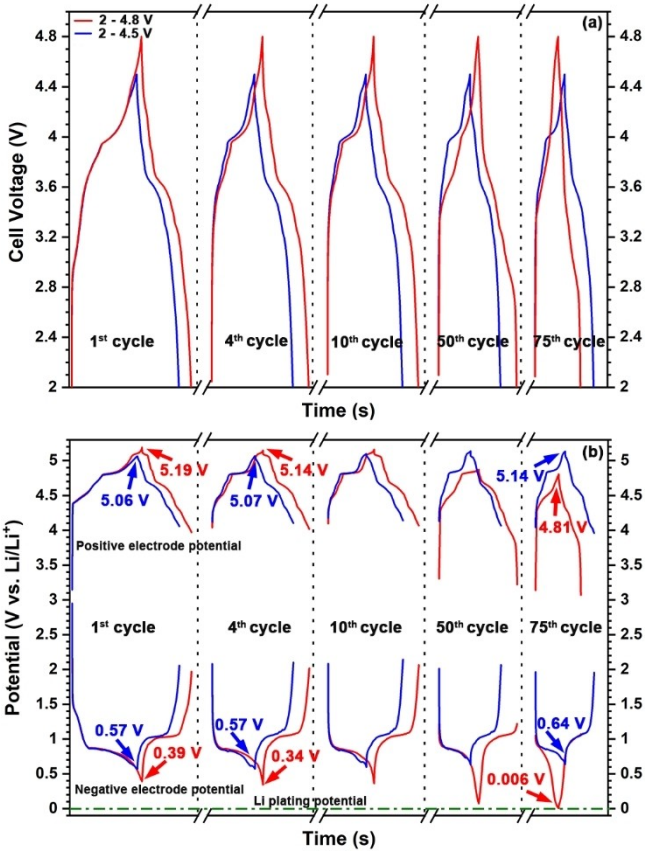

Figure 4. Cell voltage and potential profiles of individual electrodes in DIBs assembled as three-electrode cells with additional reference electrodes: (a) cell voltage as a function of time for two DIBs operating between 2 and 4.5 V and between 2 and 4.8 V, respectively; (b) potential profiles of graphite and Sb-carbon composite electrodes operated from the corresponding cells. The cells are initially charged and discharged at a current of 0.1 C (10 mA/$g_{cathode}$) for three cycles and then charged and discharged at 0.5 C (50 mA/g) for the remaining cycles in a 3.4 M LiTFSI in DMC electrolyte.

from 0.1 C to 0.5 C for the cell with a 4.5 V upper cut-off. This can be inferred from the respective electrode voltages at the end of charge during the fourth cycle. The negative electrode potential profile does not exhibit any shift, whereas a minor increase in the voltage polarisation for the graphite electrode after 75 cycles is observed (Figure 4; Table 2). Both the electrochemical performance behaviours can be explained from the C_{EFF} of the individual Li metal cells. There is a small difference in the initial C_{EFF} of the Sb-carbon composite (67.3 %) in comparison to that of the graphite electrode (75 %, as reported in our previous article).[24] The C_{EFF} of the Sb-carbon composite electrode cycled in a full potential window of 0.01–2 V was close to 98 % after a few initial cycles. In our previous reports,[24,35] we explored the behaviour of black phosphorus – carbon composite electrode and demonstrated that cyclic behaviour stabilised and and a higher C_{EFF} (99 %) was achieved when a Li metal cell was cycled within a restricted potential (0.5–2.0 V instead of 0.01–2 V vs Li|Li$^+$). These effects are likely to be caused by a reduced volume change as the initial material is not transformed to the final alloy phase. We expect that a similar phenomenon and a much improved C_{EFF} (above 98 %) can be expected for the Sb-carbon composite electrode when it operates within a restricted potential window (i.e., when the bottom cut-off potential reaches only 0.57 or 0.39 V vs Li|Li$^+$). However, the C_{EFF} of the graphite electrode is highly dependent on the upper cut-off potential. In the case of cells operating between 2 and 4.8 V, the C_{EFF} of the graphite electrode is around 96.8 %, a smaller value than that for the Sb–C composite (equal to or above 98 %). The graphite electrode suffers from stronger parasitic reactions at a higher cut-off potential (~5.2 V versus Li|Li$^+$), which can be illustrated by its low C_{EFF} under such conditions. The NE potential shifts down during continuous cycling and almost reaches 0 V vs Li|Li$^+$, demonstrating that Li$^+$ gets trapped within the material over progressive cycling. Some of the failure mechanisms of DIBs that can be relevant here are outlined in a previous publication.[34] In this

Table 1. Cut-off potentials of graphite and Sb-carbon composite electrodes in a DIB full cell operated between 2 and 4.8 V.

Cycle No	Graphite's potential (at the end of charge), V vs Li|Li$^+$	Sb-carbon composite's potential (at the end of charge), V vs Li|Li$^+$	Graphite's potential (at the end of discharge), V vs Li|Li$^+$	Sb–C composite's potential (at the end of discharge), V vs Li|Li$^+$
1	5.19	0.39	3.97	1.97
4	5.14	0.34	4.02	2.02
10	5.16	0.36	4.06	2.06
50	4.87	0.07	3.22	1.22
75	4.81	0.006	3.07	1.07

Table 2. Cut-off potentials of graphite and Sb-carbon composite electrodes in a DIB full cell operated between 2 and 4.5 V.

Cycle No	Graphite's potential (at the end of charge), V vs Li|Li$^+$	Sb-carbon composite's potential (at the end of charge), V vs Li|Li$^+$	Graphite's potential (at the end of discharge), V vs Li|Li$^+$	Sb–C composite's potential (at the end of discharge), V vs Li|Li$^+$
1	5.06	0.57	4.06	2.06
4	5.07	0.57	4.10	2.10
10	5.1	0.60	4.14	2.14
50	5.14	0.64	4.06	2.07
75	5.14	0.64	3.96	1.96

case, it is likely that a lower C_{EFF} of the PE traps the Li^+ in the NE, gradually lowering its potential. In contrast, the C_{EFF} of both the electrodes are close to identical (97.8% for the NE and slightly above 98% for the PE) in the cells operating within a voltage window of between 2 and 4.5 V, minimising potential drift in the electrodes.

The Influence of an Electrolyte Additive on the Electrochemical Performance of Sb-carbon/Graphite Full Cells

As reported previously,[24] insertion and de-insertion of anions in graphite electrodes occur at a high potential (4.2 V to 5.2 V vs Li/Li^+) via a stage-like transition, from stage IV to stage I, resulting in the formation of $(TFSI)C_{20}$ insertion compound in the end of this process (which corresponds to a capacity of 112 mAh/g). An enhanced operating voltage of a full cell leads to a higher capacity. However, it also causes detrimental performance of the electrode due to highly irreversible reactions such as oxidative decomposition of the electrolyte. To reduce the parasitic effect of the electrolyte on the electrode at a high voltage, 1% of vinylene carbonate (VC) was added to the 3.4 M LiTFSI in DMC electrolyte. The influence of the electrolyte additive on the cyclic stability of the full cells operated between 2.0–4.8 Vis shown in Figure 5(a). Two cells are assembled in a three-electrode configuration, and the average specific discharge capacity is plotted along with the standard deviation. Initially, the cells were cycled for three cycles at a slower current rate of 10 mA/g (formation cycles) and subsequently cycled at 0.5 C (50 mA/g). As mentioned in section 2.3, the displayed capacity values are based on the mass of the positive electrode. The cells achieve a discharge capacity of 52 mAh/g in the last formation cycle; the capacity reduces slightly to 49 mAh/g (fourth cycle) as the current rate is increased from 10 to 50 mA/g and then exhibits excellent capacity retention of 97.5% after 103 cycles (Figure 5a). This is in direct contrast with the cells cycled within the same voltage window in the absence of VC; even though a much higher capacity is obtained initially in the absence of VC (Figure 3a), the capacity of the full cell drops drastically from 89 mAh/g (fourth cycle) to 44 mAh/g at the end of 78 cycles, lower than the capacity of cells with the VC-containing electrolyte. The C_{EFF}s of the cells operated within the same potential window are shown in Figure 5b. A very low initial C_{EFF}, i.e., around 28.4%, is observed for the cells cycled within a voltage window of 2.0–4.8 V. Over the successive cycles, the C_{EFF} increases and reaches 97% at the end of 18 cycles and maintains a steady value until the end of the cycling period. A stable C_{EFF} is retained until the end of the 103^{th} cycle.

To gain a more detailed insight into the operation of the cells, the cell voltages of full cells and potential profiles of individual electrodes against lithium metal references are plotted in Figure 6. Cell voltages of the full cell tested in the presence and absence of an electrolyte additive are superimposed upon each other in Figure 6a. The potentials of individual electrodes for the same votlage range 2–4.8 V are shown in Figure 6b. Let us discuss the effects of the VC additive using the data. It can be seen that the addition of VC leads to an extended first charge, which is related to the oxidative decomposition of the VC at around 4.6 V on the graphite positive electrode; the positive electrode eventually reaches a potential of 4.77 V (vs $Li|Li^+$) at the end of the first charge (Figure 6b). As a result of an extended charge process, the potential of the Sb–C composite electrode shifts much lower then in the cell without an additive. Indeed, this extra alloying with lithium in the Sb–C electrode is needed to maintain charge neutrality during the extensive irreversible oxidation of VC at the graphite cathode. In the cell shown in Figure 6b, the potential briefly drops even below 0 V vs $Li|Li^+$ (down to −0.03 V versus $Li|Li^+$; Table 3 and SI Figure S6), a type of

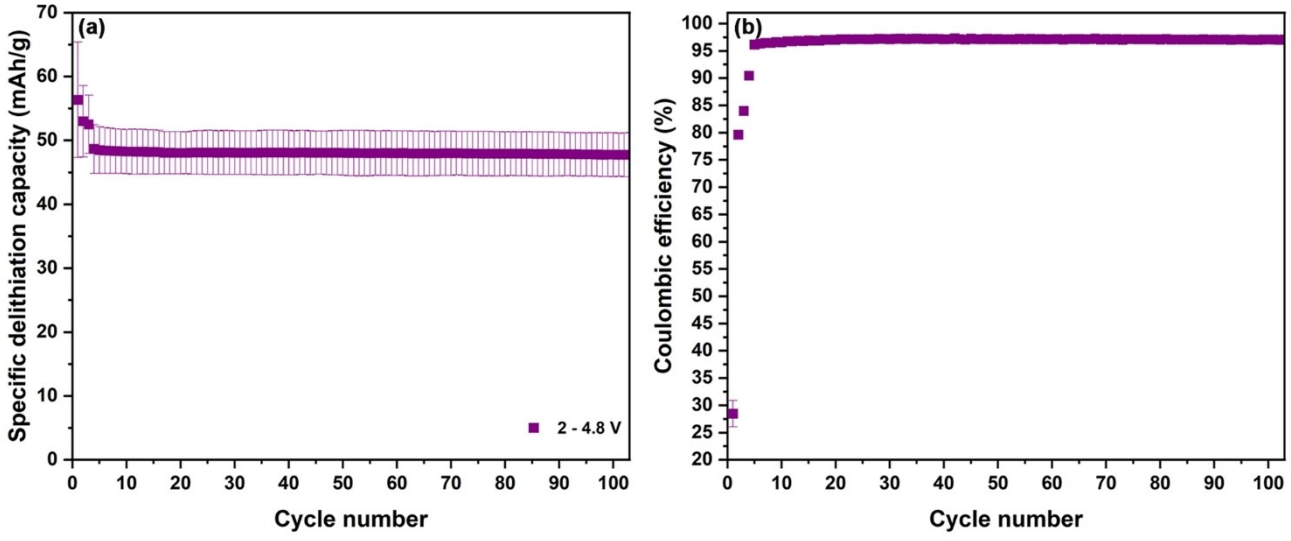

Figure 5. Electrochemical performance of graphite||Sb–C full cells tested in a three-electrode set-up using 1% VC electrolyte additive in 3.4 M LiTFSI in DMC. (a) Specific discharge capacity as a function of cycle number obtained using a constant current mode in voltage window of 2.0–4.8 V; (b) corresponding Coulombic efficiencies.

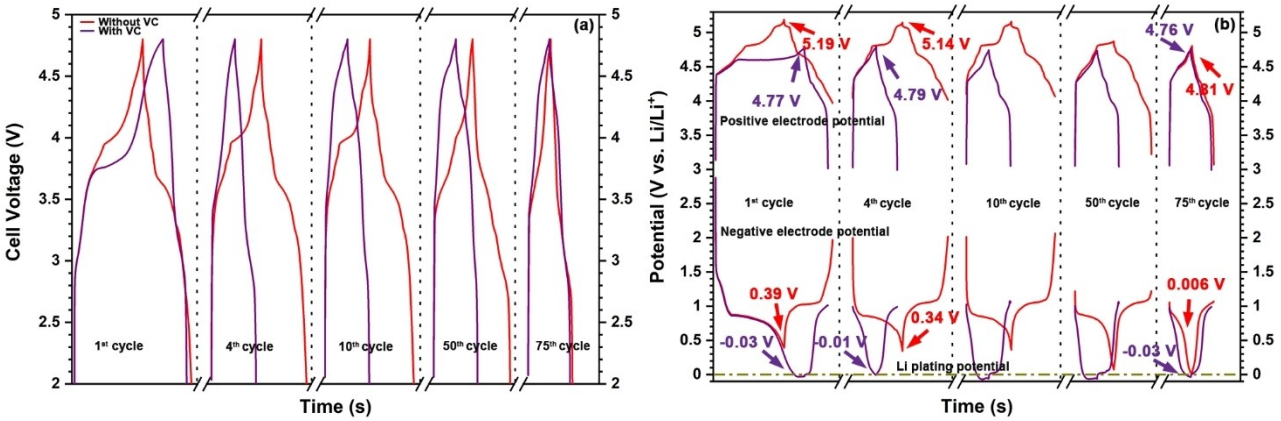

Figure 6. Charge-discharge profiles recorded from the cells operated in a three-electrode set up in the presence and absence of 1% VC as an additive in a 3.4 M LiTFSI in DMC electrolyte: (a) cell voltage as a function of time for the cell cycled within 2–4.8 V (b) potentials of graphite and Sb–C electrodes as a function of time for the corresponding cells. Colour scheme: red – cell with no additive; purple – cell with 1% VC.

Table 3. Cut-off potentials of graphite and Sb–C composite electrodes from a cell operated within 2–4.8 V using 1% VC as electrolyte additive in 3.4 M LiTFSI in DMC.

Cycle No	graphite potential (at the end of charge), V vs Li|Li$^+$	Sb–C composite potential (at the end of charge), V vs Li|Li$^+$	graphite potential (at the end of discharge), V vs Li|Li$^+$	Sb–C composite potential (at the end of discharge), V vs Li|Li$^+$)
1st cycle	4.77	-0.03	3.02	1.01
4th cycle	4.79	-0.007	2.99	0.99
10th cycle	4.74	-0.06	3.05	1.08
50th cycle	4.74	-0.06	3.04	1.06
75th cycle	4.76	-0.03	2.99	0.99

potential with a possibility of lithium plating. It should be noted that the electrode balancing in the cell can be adjusted to regulate the negative electrode lowest potential, a minor dip of the potential to the negative territory in this initial experiment can be easily corrected. The experiment is nevertheless significant to demonstrate typical effects that occur in a cell upon the VC addition to the electrolyte. Due to the large shift in the NE potential, the end of charge potential of graphite is limited to 4.77 V (versus Li|Li$^+$), which notably limits the charge capacity provided by the intercalated anions. During the discharge, in the NE, delithiation of Li from the Sb–C composite occurs (Figure 6b, S.I. Figure 6c). Due to the first cycle irreversibility in the PE, the Sb–C composite electrode still exhibits a high degree of lithiation at the end of the first discharge (1.01 V versus Li|Li$^+$). In contrast, the anions are completely de-intercalated from the PE (3.02 V vs Li|Li$^+$).

As it follows, the initial decomposition of VC at a lower potential (~4.6 V vs Li|Li$^+$) is the primary reason behind the depleted reversible capacity and reduced C_{EFF} in the first cycle. The above phenomenon is similar to that explained by Heidrich *et al.* for DIB full cells while using VC as an additive for the electrolyte previously.[34] In terms of cell stability, there are two positive outcomes. First, the upper potential of the PE never reaches the electrolyte oxidation potential (above 5.0 V) and remains stable between 4.74 and 4.79 V during its entire cyclic period, improving the cell stability. Second, the volume expansion of the Sb–C of the material is reduced due to the lower cell capacity. Therefore, an enhanced cyclic stability is achieved and an improved C_{EFF} in the later cycles is demonstrated in the cells with the VC electrolyte additive. These results indicate that VC electrolyte additive has pronounced effects on the cell operation. While it decreases the overall cell capacity, the cell's cyclic stability is markedly improved. After long cycling (such as in excess of 75 cycles), the remaining capacity in a cell with the electrolyte additive may be higher than the remaining capacity in the cell without such an additive, which experiences considerable degradation during the extensive cycling.

Energy Density Comparison of DIBs Sb-carbon Composite Electrodes and Dual Graphite DIBs

A very important metric for new batteries is their specific energy density. This was calculated for three cells (two with the new Sb–C NEs and one with a more traditional graphite NE) on the basis of their first discharge capacity, and the results are shown in Figure 7. The specific energy density is calculated in two ways, based on the mass of both electrodes (left-hand side of Figure 7) and the combination of the mass of both electrodes and salt (right-hand side of Figure 7). Based on the combined electrode masses, there is no marked difference in the energy densities of the SGDIB cell (2–4.8 V) and a dual graphite battery (DGB) (2–5.0 V), evaluated in our previous work.[24] Both cells exhibit an energy density of around 290 Wh/kg. However, the cycling stability of SGDIB deteriorates relatively quickly com-

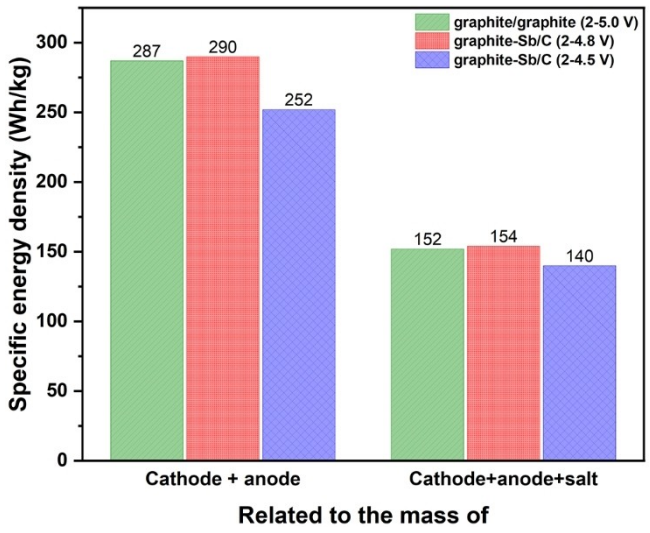

Figure 7. The specific energy density of full cells calculated from the first discharge cycle based on the mass of (left-hand side) both electrodes and (right-hand side) both electrodes and LiTFSI salt. Values for mean discharge voltage and the 1st discharge capacity for energy calculation of graphite||graphite full cells are according to our previous DIB paper.[24]

pared to the DGB[24] cell; therefore, the energy density will also decrease over the cyclic period. In order to improve the stability of SGDIB, the cells have to be operated within the reduced cell voltage window (2- 4.5 V); this however comes at a cost and the energy density of those cells is reduced to 252 Wh/kg.

Unlike the situation in LIBs, where the electrolyte's role is primarily related to cation (Li^+) transport between the two electrodes during charging and discharging, the electrolyte contributes to the capacity in DIBs. Hence, it is often considered necessary in the field of dual-ion batteries to consider the salt mass as well while calculating the cell's energy density. After including masses of all active components, the energy density of SGDIB is reduced to 154 Wh/kg, slightly higher than that of DGB. The noted decrease in the energy density of the cell is attributed to the relatively heavy mass of the $TFSI^-$ anion (280.14 g/mol), and can be in principle reduced by replacing this anion with an anion of a lower mass, such as PF_6^- or BF_4^-.[24]

Recently, we have reported another study on DIBs with NEs containing black phosphorus,[24] and it is useful to compare their specific energies with those of SGDIP cells reported here. Similar minor improvements of specific energies over those of DGBs were observed. For example, an increase in the specific energy was possible between DGBs and DIBs with phosphorus electrodes operating in a voltage window of 2–4.7 V from 287 to 319 Wh/kg (per mass of two electrodes) or from 152 to 155 Wh/kg (per mass of both electrodes and active salt). This shows that DIBs with both Sb-based and P-based NEs demonstrate comparable performance, with some improvement of specific energies over DGBs.

The reported specific energies of SGDIB cells can also be compared with Si- and Ge-based DIBs reported in the literature. Here, we can refer to two studies in which experimental details allow straightforward reproduction of experiments (e.g., electrode balancing is explained well). Li *et al.* have used nano-silicon as a NE and $LiPF_6$ as a conductive salt in the electrolyte in a cell with 1:2.2 capacity balancing between PE and NE.[36] The specific energy of the resulting cell, calculated per total mass of the two electrodes and active salt, was 185 Wh/kg (S.I. Table S3), a 20% gain in comparison with the highest energy SGDIB cell reported here. In turn, Zhou *et al.* have reported a DIB cell with a Ge–CNF composite NE and $LiPF_6$ salt, with PE:NE electrode mass balancing of 12:1.[22] The specific energy density of the cell, calculated per mass of the electrodes, was approximately 80 Wh/kg, and there was no substantial change in the energy density, apart from a minor reduction by 2 Wh/kg, when the weight of the salt was included (S.I. Table S3). A direct comparison between separate studies is however complicated by the fact that different electrode balancing, salt chemistry, operating voltages and other test parameters are used by different groups. Further analysis of DIB cells with various alloying materials (e.g., Si, Sn, or Ge) in their NEs, using consistent experimental methodology will be important for the understanding of optimal cell parameters and the improvement of cyclic stability.

Conclusions

A composite antimony-carbon (Sb–C) material synthesised using ball milling was evaluated for the first time in lithium-based DIBs, and these cells were compared with more conventional dual-graphite batteries. The electrochemical behaviour of Sb–C || Li metal cells with highly concentrated electrolytes is dependent on electrode and cell fabrication parameters. In particular, pressing the electrode and using polyolefin non-woven separators are detrimental to the cells with HCEs. The initial capacity of the unpressed electrode was 485 mAh/g at a current rate of 230 mA/g in a 3.4 M LiTFSI in DMC electrolyte using a Whatman GF/D separator, and a capacity of 285 mAh/g was retained at the end of 100 cycles. After characterising the performance of electrodes in Li metal cells, Sb–C||graphite full full-cells were designed and tested using a three-electrode setup. By operating the cells within a wider voltage window (2.0–4.8 V), a higher specific discharge capacity of 94.3 mAh/g was achieved but at the expense of cyclic stability compared to the cells cycled within a voltage range of 2.0–4.5 V. To explore a possible approach to enhance the stability of cells at a higher operating potential, an electrolyte additive (1% of vinyl carbonate) was added to HCEs. As a result, the cells displayed excellent cyclic stability with a capacity retention of 44.2 mAh/g (90.4% in comparison with the fourth cycle) over 78 cycles. Maximal observed specific energies were calculated from the Sb–C||graphite full cells. A specific energy of 290 Wh/kg related to the mass of both electrodes, similar to that of DGBs was observed. The specific energy becomes 154 Wh/kg (152 Wh/kg for DGBs) when it is calculated based on the combined mass of active salt and both electrodes. This study demonstrates the initial prorotypes of DIBs with Sb-based electrodes and advances our understanding of the choice of alloying materials available for these cells.

Experimental

Material Synthesis: Antimony (325 mesh, 99.5% purity, Johnson Matthey Electronics) and graphite (Sigma Aldrich, 282863, < 20 μm) were mixed in a 7:3 weight ratio. A 5 g of the mixture were loaded into a magneto-ball mill with four stainless steel balls (25.4 mm in diameter), and the ball to powder ratio was 52.8:1. The milling was performed under an argon (Ar) atmosphere at 100 kPa above atmospheric pressure in the presence of an external magnet at a 135 degree position with respect to the vertical direction. The milling was performed at a rotation speed of 160 rpm for 100 h. The as-milled composite powders were unloaded from the ball mill container inside an Ar filled glove box. A detailed description of the material synthesis and the working principle of magneto ball mill are reported in our previous work.[29]

Material characterisation: X-ray diffraction (XRD) pattern from the composite powder was collected using a PANalytical Empryrean instrument equipped with Cu Kα radiation ($\lambda = 1.54181$ Å). The pattern was obtained using a step size of 0.026° and step time of 400 s. The as obtained pattern was analysed using X'pert High Score Plus software. The Raman spectrum was measured using Horiba Labram system equipped with confocal optics. A 532 nm wavelength laser was used to record the spectra. The power of the laser was 1 mW, equivalent to 10% of total laser power, and a 50x lens was used in the test. The transmission electron microscopy (TEM) data and energy-dispersive x-ray (EDX) elemental maps were acquired on a JEOL JEM-2100F instrument. The specific densities of Sb–C composite and super P C65 were acquired using Micromeritics AccuPyc II and Anton Paar ultrapyc 5000 Helium pycnometers, respectively. The electrode porosity was calculated using Equation 1:[37]

$$\text{Porosity} = \frac{L - W((C1/D1) + (C2/D2) + (C3/D3))}{L}, \quad (1)$$

where L is the real thickness of the electrode in cm; W is the weight of the electrode (excluding the weight of the foil) in g/cm^2; C1, C2, and C3 represent the weight percentage of the active material, carbon black, and binder, respectively. D1, D2, and D3 represent the true density in g/cm^3 of the active material, carbon black, and binder, respectively.

Electrochemical characterisation: Graphite electrodes with a mass loading of 3.8–4.4 mg cm^{-2} were composed of 90 wt% KS6 graphite (Imerys), 5 wt% sodium carboxymethyl cellulose (Na–CMC) binder (Walocel CRT 2000 PPA12, Dow Wolff Cellulosics) and 5 wt% conductive carbon (C-NERGY Super C65). Aluminum foil (Evonik Industries, 15 μm thickness) served as current collector. Antimony-carbon composite electrodes were prepared using the mass ratio of 80% of the active material, 10% of conductive carbon, and 10% of sodium carboxymethyl cellulose (Na–CMC) binder. The average mass loading of Sb–C electrode used in Sb||Li metal cells was 1.3 ± 0.3 mg/cm^2. For graphite||Sb/C full cells, the average mass loading to achieve a N/P capacity balancing of ≈1.1–1.2 was 0.7 ± 0.1 mg/cm^2. Electrochemical measurements were performed in stainless steel two-electrode coin cells (CR2032) or stainless steel three-electrode T-type cells (Swagelok). For the two-electrode coin cells, Li metal negative electrodes and Sb–C positive electrodes with a diameter of 12 mm were used to investigate the performance of Sb–C with different electrolytes. The electrodes were separated by a glass microfiber separator (Whatman filter, grade GF/D, ø = 13 mm) or a three-layered PP fleece separator (FS2226, Freudenberg, ø = 13 mm) which was soaked with 120 μL electrolyte. Three-electrode T-type cells consisting of a Li metal reference electrode (RE; ø = 5 mm), an Sb–C anode, a graphite cathode (ø = 12 mm) and a glass microfiber separator (Whatman filter, grade GF/D, ø = 13 mm); full-cell setup; control of cell voltage) were used to additionally monitor the electrode potentials during full cell cycling. Constant current charge–discharge cycling was performed on a Maccor 4000 battery test system at 20 °C. Two-electrode Sb–C||Li metal cells were cycled at 0.2 C for three cycles (1 C = 574 mA/g, based on the theoretical capacity of the Sb–C composite). Subsequently, cycling was performed at 0.4 C. Three-electrode graphite||Sb–C full cells were initially cycled for three cycles (2.0–4.5 V or 2.0–4.8 V) with a constant current of 0.1 C (1 C = 100 mA/g based in the practical capacity of KS6 graphite electrodes for anion insertion). During cycling, the cell voltage was used for setting up cycling limits. Following cycles were performed at a current of 0.5 C.

Acknowledgements

This work was supported through a Discovery Project (DP210102806) awarded by the Australian Research Council and the Australia–Germany Joint Research Cooperation Scheme (an initiative between Universities Australia and the German Academic Exchange Service (DAAD)). The work also received the support from the Australian Research Council (ACT, ACT, AU) Australian Research Hub, grant number IH200100035. The German authors thank the DAAD for funding (57446388) within this initiative. The authors also thank the Ministry of Economic Affairs, Innovation, Digitalization and Energy of the State of North Rhine-Westphalia (MWIDE) for funding this work in the project "GrEEn" (313-W044 A). The authors acknowledge the facilities and the scientific and technical assistance of Microscopy Australia at the Advanced Imaging Precinct, Australian National University, a facility that is funded by the University, and State and Federal Governments. The authors acknowledge Dr. Neeraj Mishra (Anton Paar Australia Pty. Ltd., Sydney) and Dr. Michael Turner (Research School of Physics, the Australian National University) for the assistance in measuring the true density of materials and Mr. Ary A. Wibowo and Dr. Hieu T. Nguyen for their help with Raman measurements. Open Access publishing facilitated by Australian National University, as part of the Wiley - Australian National University agreement via the Council of Australian University Librarians.

Conflict of Interests

The authors declare no conflict of interest.

Data Availability Statement

The data that support the findings of this study are available from the corresponding author upon reasonable request.

Keywords: alloying · anion intercalation · antimony · dual-ion batteries · graphite

[1] The Electric Vehicle World Sales Database. http://www.ev-volumes.com/.
[2] Global Energy Review IEA (2021), IEA, Paris. http://www.iea.org/reports/global-energy-review-2021.
[3] N. Tapia-Ruiz, A. R. Armstrong, H. Alptekin, M. A. Amores, H. Au, J. Barker, R. Boston, W. R. Brant, J. M. Brittain, Y. Chen, M. Chhowalla, Y.-S. Choi, S. I. R. Costa, M. Crespo Ribadeneyra, S. A. Cussen, E. J. Cussen, W. I. F. David, A. V. Desai, S. A. M. Dickson, E. I. Eweka, J. D. Forero-Saboya, C. P. Grey, J. M. Griffin, P. Gross, X. Hua, J. T. S. Irvine, P. Johansson, M. O. Jones, M. Karlsmo, E. Kendrick, E. Kim, O. V. Kolosov, Z. Li, S. F. L. Mertens, R. Mogensen, L. Monconduit, R. E. Morris, A. J. Naylor, S. Nikman, C. A. O'Keefe, D. M. C. Ould, R. G. Palgrave, P. Poizot, A. Ponrouch, S. Renault, E. M. Reynolds, A. Rudola, R. Sayers, D. O. Scanlon, S. Sen, V. R. Seymour, B. Silván, M. T. Sougrati, L. Stievano, G. S. Stone, C. I. Thomas, M.-M. Titirici, J. Tong, T. J. Wood, D. S. Wright, R. Younesi, *J. Phys. Energy* **2021**, *3*, 031503.
[4] T. Hosaka, K. Kubota, A. S. Hameed, S. Komaba, *Chem. Rev.* **2020**, *120*, 6358–6466.
[5] B. Ji, H. He, W. Yao, Y. Tang, *Adv. Mater.* **2021**, *33*, 2005501.
[6] X. Xu, K. S. Hui, K. N. Hui, J. Shen, G. Zhou, J. Liu, Y. Sun, *Chem. Eng. J.* **2021**, *418*, 129385.
[7] A. Medina, C. Pérez-Vicente, R. Alcántara, *Mater.* **2021**, *14*, 7488.
[8] T. Placke, A. Heckmann, R. Schmuch, P. Meister, K. Beltrop, M. Winter, *Joule* **2018**, *2*, 2528–2550.
[9] W. Rüdorff, U. Hofmann, *Z. Anorg. Allg. Chem.* **1938**, *238*, 1–50.
[10] a) L. Zhang, H. Wang, X. Zhang, Y. Tang, *Adv. Funct. Mater.* **2021**, *31*, 2010958; b) É. Deunf, P. Jiménez, D. Guyomard, F. Dolhem, P. Poizot, *Electrochem. Commun.* **2016**, *72*, 64–68; c) W. Ma, L.-W. Luo, P. Dong, P. Zheng, X. Huang, C. Zhang, J.-X. Jiang, Y. Cao, *Adv. Funct. Mater.* **2021**, *31*, 2105027.
[11] a) S. Dühnen, R. Nölle, J. Wrogemann, M. Winter, T. Placke, *J. Electrochem. Soc.* **2019**, *166*, A5474; b) C. Li, H. Yang, J. Xie, K. Wang, J. Li, Q. Zhang, *ACS Appl. Mater. Interfaces* **2020**, *12*, 32719–32725.
[12] K.-H. Kwak, H. J. Suh, A. Kim, S. Park, J. Song, S. Li, Y. Kim, G. Jeong, H. Kim, Y.-J. Kim, *Nano Energy* **2019**, *66*, 104138.
[13] a) T. Ishihara, M. Koga, H. Matsumoto, M. Yoshio, *Electrochem. Solid-State Lett.* **2007**, *10*, A74; b) A. Heckmann, J. Thienenkamp, K. Beltrop, M. Winter, G. Brunklaus, T. Placke, *Electrochim. Acta* **2018**, *260*, 514–525.
[14] a) S. Zhao, Y. Huang, Y. Wang, D. Zhu, L. Zhang, H. Wang, *ACS Appl. Energ. Mater.* **2021**, *4*, 737–744; b) J. Gao, M. Yoshio, L. Qi, H. Wang, *J. Power Sources* **2015**, *278*, 452–457.
[15] T. Fukutsuka, F. Yamane, K. Miyazaki, T. Abe, *J. Electrochem. Soc.* **2016**, *163*, A499.
[16] P. Meister, V. Siozios, J. Reiter, S. Klamor, S. Rothermel, O. Fromm, H.-W. Meyer, M. Winter, T. Placke, *Electrochim. Acta* **2014**, *130*, 625–633.
[17] J. Gao, S. Tian, L. Qi, H. Wang, *Electrochim. Acta* **2015**, *176*, 22–27.
[18] C.-M. Park, J.-H. Kim, H. Kim, H.-J. Sohn, *Chem. Soc. Rev.* **2010**, *39*, 3115–3141.
[19] Top Silicone Anode Companies (Venture Radar). http://www.venturer-adar.com/keyword/Silicon%20anode.
[20] J. Li, A. K. Dozier, Y. Li, F. Yang, Y.-T. Cheng, *J. Electrochem. Soc.* **2011**, *158*, A689.
[21] a) S. Wang, X. Xiao, Y. Zhou, C. Fu, S. Jiao, *Electrochim. Acta* **2018**, *282*, 946–954; b) S. He, S. Wang, H. Chen, X. Hou, Z. Shao, *J. Mater. Chem. A* **2020**, *8*, 2571–2580; c) C. Jiang, L. Xiang, S. Miao, L. Shi, D. Xie, J. Yan, Z. Zheng, X. Zhang, Y. Tang, *Adv. Mater.* **2020**, *32*, 1908470.
[22] J. Zhou, Y. Zhou, X. Zhang, L. Cheng, M. Qian, W. Wei, H. Wang, *Nanoscale* **2020**, *12*, 79–84.
[23] a) X. Zhang, Y. Tang, F. Zhang, C.-S. Lee, *Adv. Energy Mater.* **2016**, *6*, 1502588; b) X. Tong, F. Zhang, G. Chen, X. Liu, L. Gu, Y. Tang, *Adv. Energy Mater.* **2018**, *8*, 1701967; c) C. Song, Y. Li, H. Li, T. He, Q. Guan, J. Yang, X. Li, J. Cheng, B. Wang, *Nano Energy* **2019**, *60*, 285–293.
[24] J. M. Wrogemann, L. Haneke, T. Ramireddy, J. E. Frerichs, I. Sultana, Y. I. Chen, F. Brink, M. R. Hansen, M. Winter, A. M. Glushenkov, T. Placke, *Adv. Sci.* **2022**, *9*, 2201116.
[25] C.-M. Park, S. Yoon, S.-I. Lee, J.-H. Kim, J.-H. Jung, H.-J. Sohn, *J. Electrochem. Soc.* **2007**, *154*, A917.
[26] a) J. S. Lannin, J. M. Calleja, M. Cardona, *Phys. Rev. B* **1975**, *12*, 585–593; b) X. Wang, K. Kunc, I. Loa, U. Schwarz, K. Syassen, *Phys. Rev. B* **2006**, *74*, 134305.
[27] T. Ramireddy, N. Sharma, T. Xing, Y. Chen, J. Leforestier, A. M. Glushenkov, *ACS Appl. Mater. Interfaces* **2016**, *8*, 30152–30164.
[28] S. Miyoshi, H. Nagano, T. Fukuda, T. Kurihara, M. Watanabe, S. Ida, T. Ishihara, *J. Electrochem. Soc.* **2016**, *163*, A1206–A1213.
[29] T. Ramireddy, M. M. Rahman, T. Xing, Y. Chen, A. M. Glushenkov, *J. Mater. Chem. A* **2014**, *2*, 4282–4291.
[30] a) G. Jiang, F. Li, H. Wang, M. Wu, S. Qi, X. Liu, S. Yang, J. Ma, *Small Structures* **2021**, *2*, 2000122; b) Y. Yamada, J. Wang, S. Ko, E. Watanabe, A. Yamada, *Nat. Energy* **2019**, *4*, 269–280.
[31] a) N. Ehteshami, E. Paillard, *ECS Trans.* **2017**, *77*, 11–20; b) M. Nie, D. Chalasani, D. P. Abraham, Y. Chen, A. Bose, B. L. Lucht, *J. Phys. Chem. C* **2013**, *117*, 1257–1267; c) S. K. Heiskanen, J. Kim, B. L. Lucht, *Joule* **2019**, *3*, 2322–2333.
[32] M. Kirchhöfer, J. von Zamory, E. Paillard, S. Passerini, *Int. J. Mol. Sci.* **2014**, *15*, 14868–14890.
[33] J. Kasnatscheew, T. Placke, B. Streipert, S. Rothermel, R. Wagner, P. Meister, I. C. Laskovic, M. Winter, *J. Electrochem. Soc.* **2017**, *164*, A2479–A2486.
[34] B. Heidrich, A. Heckmann, K. Beltrop, M. Winter, T. Placke, *Energy Storage Mater.* **2019**, *21*, 414–426.
[35] T. Ramireddy, T. Xing, M. M. Rahman, Y. Chen, Q. Dutercq, D. Gunzelmann, A. M. Glushenkov, *J. Mater. Chem. A* **2015**, *3*, 5572–5584.
[36] C. Li, Y. Ju, H. Yoshitake, M. Yoshio, H. Wang, *Mater. Today Energy* **2018**, *8*, 174–181.
[37] H. Zheng, L. Tan, G. Liu, X. Song, V. S. Battaglia, *J. Power Sources* **2012**, *208*, 52–57.

Manuscript received: March 28, 2023
Revised manuscript received: July 26, 2023
Version of record online: August 22, 2023